PCCP

RSC Publishing

PAPER

View Article Online
View Journal | View Issue

Cite this: *Phys. Chem. Chem. Phys.*, 2013, **15**, 18688

Nitrogen-doped pyrolytic carbon films as highly electrochemically active electrodes†

Hugo Nolan,[ab] Niall McEvoy,[a] Gareth P. Keeley,[ab] Stephen D. Callaghan,[ac] Cormac McGuinness[ac] and Georg S. Duesberg*[ab]

Received 20th August 2013,
Accepted 25th September 2013

DOI: 10.1039/c3cp53541j

www.rsc.org/pccp

Nitrogen-doped Pyrolytic Carbon (N-PyC) films were employed as an electrode material in electrochemical applications. PyC was grown by *via* non-catalysed chemical vapour deposition and subsequently functionalised *via* exposure to ammonia–hydrogen plasma. The electrochemical properties of the N-PyC films were investigated using the ferri/ferro-cyanide and hexaamine ruthenium(III) chloride redox probes. Exceptional electron transfer properties were observed and quantified for the N-PyC compared to the as-grown films. X-ray photoelectron spectroscopy confirmed the presence of nitrogen in edge plane graphitic configurations and the surface of the N-PyC was investigated using scanning electron microscopy and atomic force microscopy. The excellent electrochemical performance of the N-PyC, in addition to its ease of preparation, renders this material ideal for applications in electrochemical sensing.

Introduction

Recent years have seen vast amounts of research being conducted in the use of various carbon-based electrodes for electrochemical applications.[1] Features such as a wide potential window, chemical, mechanical and thermal stability and good electrical conductivity[2,3] make graphitic carbon materials very attractive for many electrochemical applications such as sensing and energy conversion and storage. Materials such as glassy carbon and highly oriented pyrolytic graphite have been studied for some time and their electrochemical properties have been thoroughly established. The last 15–20 years have seen carbon allotropes such as Carbon Nanotubes (CNTs)[4] and graphene[5] utilised in various modern electrochemical applications. In this time, these carbon nanomaterials have dominated the literature and interest in other nanostructured carbon materials, such as Pyrolytic Carbon (PyC)[6] and Pyrolysed Photoresist Films (PPF),[7] has somewhat waned.

Nitrogen doping (N-doping) of graphitic materials is currently an area of great interest in the research community. Many works have dealt with various approaches to the functionalisation of CNTs[8] and graphene[9] using methods both *in situ* during synthesis[10] and *ex situ* post-synthesis.[11] N-doping of carbon materials has been shown to be of great use in the field of electrochemical energy storage and conversion. In lithium-ion (Li-ion) batteries the use of N-doped carbon *versus* pure carbon materials shows greater cycling stability for intercalation of Li-ions into the carbon lattice.[12] N-doped carbon has been shown to be an alternative to expensive noble metal catalysts for the Oxygen Reduction Reaction (ORR) in hydrogen fuel cells.[13] The biocompatibility of both CNTs and graphene has shown to be enhanced through N-doping[14] and electrochemical sensors based on these materials have shown an increased sensitivity compared to pure carbon materials.[15,16] N-doping of less exotic carbon materials has also been investigated for various applications. N-doped activated carbon has been shown to improve the adsorption of SO_2 and NO gas for scrubbing of exhaust fumes.[17,18]

PyC, formed through the pyrolysis and subsequent Chemical Vapour Deposition (CVD) of hydrocarbon precursors,[19] exhibits many of the desirable features of other graphitic materials while not suffering from arduous synthesis and handling issues that are involved with materials like CNTs and graphene. PyC has been employed in many differing applications such as in medical prosthesis,[20] as a cytocompatibility coating in medical applications[21] and as a moderator in nuclear reactors.[22] Its electrical properties have seen PyC used as vertical interconnects,[23] in Schottky barrier diodes[24] and in metal–insulator–silicon capacitors.[25] Despite its properties suited to electrochemical applications, such as good conductivity, chemical stability and wide potential window, pristine PyC exhibits rather poor charge transfer properties; limiting its use in certain areas of electrochemical

[a] *Centre for Research on Adaptive Nanostructures and Nanodevices (CRANN) & Advanced Materials Bio-Engineering Research Centre (AMBER), Trinity College Dublin, Dublin 2, Ireland. E-mail: duesberg@tcd.ie*
[b] *School of Chemistry, Trinity College Dublin, Dublin 2, Ireland*
[c] *School of Physics, Trinity College Dublin, Dublin 2, Ireland*

† Electronic supplementary information (ESI) available: Raman spectroscopy, further XPS analysis and further electrochemical measurements of N-PyC. See DOI: 10.1039/c3cp53541j

sensing. In spite of this, some studies have successfully employed PyC as the electrode material in the electrochemical detection of trace metals.[26] Modified PyC has been utilised as an electrode material *via* the *in situ* CVD of N- and B-doped PyC on porous substrates with appropriate heteroatom precursors.[27] Furthermore, porous N-doped PyC-like material has been synthesised *via* the pyrolysis of nitrogen-bearing organic compounds on mesoporous templates and successfully employed as an electrode material for ORR.[28] Recently, it has been demonstrated that PyC can be modified using a simple plasma processing step which drastically improves the electrochemical activity of the material.[29] Exposing a PyC film to reactive oxygen plasma was found to expose a greater density of active edge-plane graphitic sites and crystalline defects compared to inert basal-plane sites. In addition, it is proposed that the oxygen functionalisation which results from the treatment further facilitate charge transfer processes when characterised using redox electrochemistry. This oxygen plasma treated PyC was shown to be suitable as the electrode material in simultaneous electrochemical sensing of dopamine and paracetamol.[30]

Herein we present work on nitrogenation of PyC films *via* exposure to a downstream ammonia–hydrogen (NH_3–H_2) plasma mixture. The NH_3 radicals reacted with the carbon films to create nitrogen functional groups on the surface of the PyC. N-doping of the PyC was confirmed *via* spectroscopic techniques; such samples are henceforth referred to as N-PyC. It is noteworthy that both processes, PyC growth and N-doping, are cost-effective and scalable. Our electrochemical investigations revealed exceptionally good electron transfer properties of the N-PyC with ferri/ferro-cyanide and hexaamine ruthenium(III) chloride redox probes.

Experimental

All chemicals used were purchased from Sigma-Aldrich and used as-received. Purified water (18 MΩ) from a Barnstead Nanopure system was used to make all aqueous solutions. For the electrochemical measurements, a Gamry Reference 600 potentiostat was used in conjunction with a three-electrode cell configuration. The PyC sample was employed as the working electrode in this set-up in the same manner as previously reported.[19,29,30] The PyC sample chip was encased in a home-made assembly whereby a disc of PyC of radius 1.5 mm was exposed to the electrolyte. Pt wire and Ag/AgCl were used as the counter and reference electrodes, respectively. For Electrochemical Impedance Spectroscopy (EIS) an AC frequency was applied in the range of 10^5 to 10^{-1} Hz at a potential of +0.26 V.

Samples of PyC were grown on SiO_2 *via* on non-catalysed CVD process whereby acetylene was thermally decomposed at 950 °C in a Gero quartz tube furnace. Growth time was 30 minutes at ~180 sccm C_2H_2 flow at a pressure of 20 Torr to yield films of a thickness of ~400 nm. Samples were cooled to room temperature under inert atmosphere to ensure minimal surface functionalisation with oxygen. Discussion of the various parameters is dealt with in greater detail in a previous work on this material.[19] Plasma treatments were carried out in a R^3T TWR-2000 T microwave radical generator with an equal gas mixture of NH_3 and H_2 (both 50 sccm) at a pressure of ~600 mTorr and a power of 1 kW. Samples were placed at a location remote from the plasma source itself, ensuring that plasma was not ignited directly over the sample. This reduced kinetic damage from accelerated ions and allowed excited radicals to react with the sample in a ''chemical plasma''. Exposure times of 45 minutes were used for the plasma treated samples in this report. The effect of different plasma treatment times on the properties of the N-PyC was also investigated. Details on this are included in the ESI† which accompanies this paper. The plasma treatment process described here has previously been shown to be suitable for the plasma treatment and functionalisation of extremely fragile graphene films[31,32] and has successfully been used in the reduction and N-doping of graphene oxide powder.[33]

X-ray Photoelectron Spectroscopy (XPS) was carried out using a monochromated Al Kα source in conjunction with an Omicron EA 125 hemispherical analyser. Combined instrumental and source resolutions for C 1s and N 1s regions with pass energy of 20 eV were ~0.55 eV. Scanning Electron Microscopy (SEM) was carried out in a Carl Zeiss Ultra FE SEM with an in-lens detector employed. Atomic Force Microscopy (AFM) measurements were completed using an Asylum MFP-3D AFM in AC mode. Raman spectroscopy was performed using a Witec Alpha 300 R confocal scanning Raman microscope with a laser wavelength of 532 nm. Raman spectra presented in this publication were averaged over 10 000 discrete spectra measured over a 30 × 30 μm area of the sample.

Results and discussion

Physical characterisation

The effect of the plasma treatment on the PyC films was investigated by characterising the surface morphology of the samples. SEM images in Fig. 1 show that, after plasma treatment, all of the samples display a greater surface roughness due to opening of the material's porous structure. This increase in roughness after plasma treatment was quantified using AFM and it was found that the RMS roughness of the as-grown PyC increased from 0.5 nm to 3.8 nm for N-PyC.

Shown in Fig. 2 are water contact angles for as-grown and N-PyC samples. The difference between the samples is stark and this is attributed to the differing functional groups on the surfaces of the two samples. The as-grown PyC displays highly hydrophobic character while the N-PyC shows a significant decrease in hydrophobicity compared to the pristine sample. Functional groups with polar character are introduced on to the PyC surface after plasma treatment and these interact with the polar water molecules to decrease the contact angle.

X-ray photoelectron spectroscopy

XPS was performed to probe the chemical nature of the N-PyC films. Spectra shown in Fig. 3 below illustrate the differing chemical composition of the surfaces of the different samples. Survey scans of the as-grown PyC and N-PyC films in Fig. 3(a)

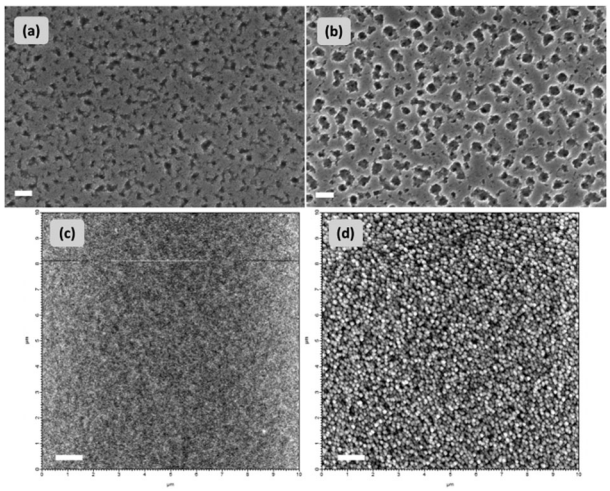

Fig. 1 SEM images of (a) as-grown PyC and (b) N-PyC. Scale bar is 200 nm in each picture. AFM images corresponding to the same samples; (c) as-grown PyC and (d) N-PyC, respectively. Scale bar is 1 μm.

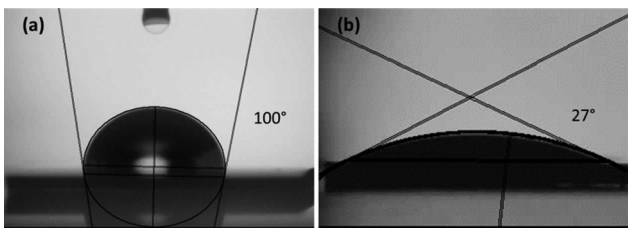

Fig. 2 Water contact angles of (a) as-grown PyC and (b) N-PyC films showing significantly increased hydrophilic character after plasma treatment; signifying changes in surface chemistry.

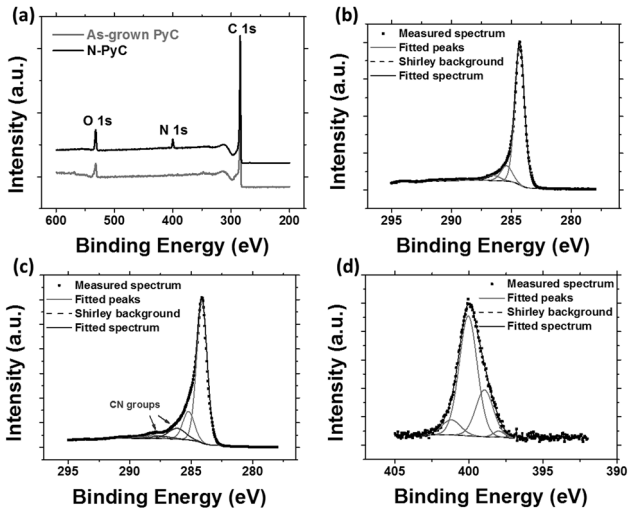

Fig. 3 (a) XPS survey scan showing spectra for as-grown PyC and N-PyC. Characteristic peaks are marked. (b) C 1s core level spectrum for as-grown PyC with spectral contributions fitted. (c) C 1s core level spectrum for N-PyC indicating new spectral contributions. (d) N 1s spectrum for N-PyC showing spectral features.

show significant differences in surface chemistry. The introduction of the N 1s peak after plasma treatment confirms N-doping of the samples. The O 1s peak present in both samples is attributed to edge termination of the graphitic crystallites in the PyC films and a certain level is inevitable. High resolution scans of the C 1s spectral region for the samples allowed different spectral contributions to be fitted to give a quantitative measure of the level of functionalisation present. The dominant feature of the C 1s region is a peak centred at ~284.4 eV;[34,35] this is due to the presence of carbon in an sp^2 or graphitic configuration. A second peak found at ~285.5 eV arises due to the presence of sp^3-hybridised carbon in the sample.[35] The PyC samples in this study display predominantly graphitic character with a narrow C 1s peak width and minimal sp^3 carbon present. This is attributed to some edge sites in the graphitic lattice as well as the presence of some covalent bonding between adjacent crystallites. A shoulder is present in the higher binding energy portion of the C 1s region and arises due to the presence of various carbon functional groups. The previously mentioned small amount of oxygen in the PyC films is present in several moieties such as hydroxyl (286.6 eV),[9,36,37] carbonyl (288 eV)[9,35] and carboxyl (289 eV)[16] groups. After NH_3–H_2 plasma treatment, new features are introduced in the C 1s region which are attributed to carbon–nitrogen groups in sp^2 (286.1 eV) and sp^3 (287.3 eV) configurations.[9] These new peaks are indicated in Fig. 3(a). The peaks due to functional groups which were present before plasma treatment are still present in the same spectral positions afterwards. It was found that the nitrogen was incorporated into the surface of the PyC film to a level of 4%, according to the survey scans. In addition, it was determined that the oxygen content of the N-PyC was not appreciably changed compared to the as-grown film. Due to this invariance it is deemed that the oxygen present bears little or no influence on the enhanced electrochemical response of the N-PyC when compared to that of the as-grown films. Further analysis of the O 1s spectral region for as-grown and N-PyC is presented in the ESI.† As XPS is a surface sensitive technique, these figures only relate to the top 2–5 nm of the film. This information is sufficient, however, as electrochemical processes only involve the electrode surface so discerning the exact chemical nature of the bulk of the PyC film is irrelevant for this study.

Further insight regarding the nature of the nitrogen functional groups was garnered by fitting spectral contributions to the N 1s region of the N-PyC sample. It was found that nitrogen is present in mostly pyrrolic (~400.1 eV)[9,11] and pyridinic (~399 eV)[9,16,38,39] configurations with small amounts of quaternary nitrogen (401 eV)[9,11,16,40] and some amine groups (397.9 eV).[41,42] That the majority of the nitrogen is present in pyridinic or pyrrolic form suggests that the NH_3–H_2 plasma treatment introduces nitrogen functional groups along the edges of the graphitic lattice of the PyC. It has been argued that for many electrochemical applications of N-doped carbon materials, nitrogen incorporated into edge sites of the graphitic lattice show the highest electrochemical activity.[1,15] Thus, such configurations are most desirable for applications exploiting this doping.

Electrochemical characterisation

Several redox probes were employed to characterise the electrochemical properties of the PyC films. Kinetics of charge transfer

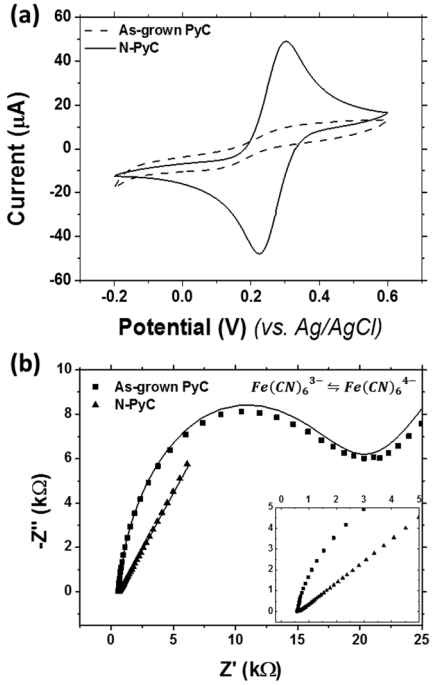

Fig. 4 (a) Voltammetric response of as-grown and plasma treated PyC in 1 mM ferri/ferro-cyanide in 1 M KCL background electrolyte. Scan rate is 100 mV s^{-1}. (b) Nyquist plots for the same system when measured using electrochemical impedance spectroscopy at a dc potential of +0.26 V. Inset: rescaled nyquist plot enlarging the region pertinent to N-PyC.

were investigated and used to gain an insight into the chemistry at the electrode surface. The ferri/ferro-cyanide redox probe was employed to this end. The electron transfer kinetics of this inner-sphere redox probe are known to be heavily influenced by the presence of different functional groups and crystalline defects on the surface of carbon electrodes.[43,44] Shown in Fig. 4 are voltammograms for as-grown PyC and N-PyC films. The peak definition for the as-grown film is very poor; indicative of rather sluggish charge transfer behaviour. In fact, so poor is the peak definition that the potential at which redox peaks are positioned cannot be identified. The plasma treated N-PyC shows a considerably different voltammetric response; a significantly better peak definition with a small peak to peak separation (ΔE_p = 71.7 mV) is observed. The heterogeneous electron transfer rate constant (k^0) gives a quantitative measure of the electron transfer behaviour and this was calculated using the Nicholson method;[45] which has been dealt with in more detail elsewhere.[46] The lack of clear peak definition for the as-grown PyC film precluded the possibility of calculating k^0 for this sample, so sluggish was the electron transfer behaviour. The N-PyC displays highly facile electron transfer with a calculated value of k^0 = 0.044 cm s^{-1}. The value of k^0 obtained here indicates that the N-PyC displays electron transfer kinetics faster even than those reported for oxygen plasma treated PyC by Keeley *et al.*[29]

Further investigations of the PyC samples using the ferri/ferro-cyanide redox probe were carried out using EIS. The results are presented as the dotted data series in the Nyquist plot in Fig. 4. Randles equivalent circuit fitting allowed the electrode–electrolyte interface to be modelled according to the measured data.[47] The solid lines in Fig. 4(b) represent the fitted data. Resistance to charge transfer (R_{ct}) values were calculated from the diameter of the semi-circular region of the Nyquist plot for the as-grown and N-PyC samples. These were found to be R_{ct} = 10 kΩ and R_{ct} = 0.16 kΩ, respectively. This is indicative of much faster electron transfer kinetics for the N-PyC electrode and is consistent with the higher k^0 calculated from the cyclic voltammetry when compared to the as-grown film.

The enhanced electrochemical performance of the N-PyC film is attributed to two reasons. As is evident from characterisation of the physical morphology (SEM, AFM, see ESI†) of the samples, the plasma treatment reactively etches a small amount of material from the surface. This increase in surface roughness exposes a greater density of edge plane graphitic sites compared to the as-grown PyC which are more electrochemically active than the basal plane graphitic sites.[48] This effect is also true for the oxygen treated PyC and has been reported on several previous occasions.[29] However, as shown here, the N-PyC displays superior electrochemical behaviour to oxygen treated samples, suggesting that the nature of the dopant atoms is of import and that N-doping, in particular, provides a route towards highly active electrode materials for electroanalytical applications. An important consideration is that the increased wettability of the N-PyC compared to the as-grown film coupled with its increased porosity. It is likely that this combination allows the analyte greater access to the electrode which will contribute towards some of the observed increase in the transferred charge in N-PyC. It is hard to deconvolute this effect from increase in redox current due to the enhanced charge transfer kinetics, but it is likely that most of the increase in peak redox current is due to charge transfer kinetics given that the electrochemical surface area of the N-PyC film does not increase compared to the as-grown film given the roughness of the samples in this study (see below).

Additional electrochemical measurements were completed using the hexaamine ruthenium(III) chloride redox probe. Cyclic voltammograms for this probe are shown in Fig. 5(a); indicating that the electron transfer kinetics are similar for both samples. This probe is well known to display ideal outer-sphere electron transfer behaviour which is not influenced by the presence of surface functional groups[49] and this behaviour is observed here; where the different surface chemistries of the PyC films bears no influence on their respective voltammetric responses. The linear relationship found to exist between the square root of the scan rate ($\sqrt{\nu}$) and the peak redox current (i_p) signifies that all redox reactions observed occur in the solution phase and the redox events are diffusion controlled processes, according to the Randles–Sevcik equation for solution-based Nernstian redox events. It is possible that the slightly higher observed peak redox current for N-PyC in this probe compared to that of as-grown PyC arises due to the presence of additional faradaic processes at the surface functional groups themselves. Indeed, the inset voltammogram in Fig. 5(a) shows the voltammetric response of as-grown PyC and N-PyC in 1 M KCl background electrolyte. The presence of small redox peaks suggests

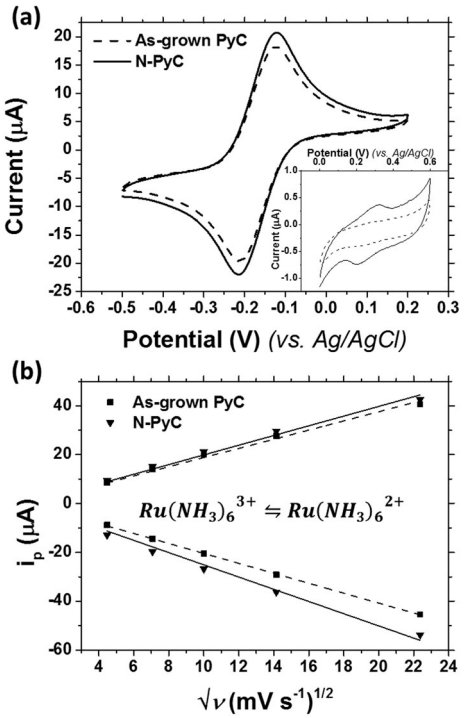

Fig. 5 (a) Voltammetric response for as-grown PyC and N-PyC films in 1 mM hexamine ruthenium(III) chloride in 1 M KCL background electrolyte. Scan rate is 100 mV s^{-1}. (b) Plots of $\sqrt{\nu}$ *versus* peak redox current (i_p) for the same samples. Data is taken from voltammetry at a range of scan rates. Inset: voltammetric response for the same sample set in 1 M KCl background electrolyte. Scan rate is 20 mV s^{-1}.

that some redox events are occurring at the surface groups in the absence of any redox active species in solution. This small pseudocapacitive behaviour contributes to the observed redox current of the system. An increase in electrochemical surface area due to roughening of the PyC surface after plasma treatment can be discounted as the observed roughness of the N-PyC film, as measured by AFM, is orders of magnitude smaller than the diffusion zone at the electrode surface.

Conclusions

A mixture of hydrogen and ammonia plasma was successfully employed to create N-groups on the surface of PyC films. This was confirmed by XPS with the emergence of a characteristic N 1s peak after the plasma treatment. Analysis of C 1s core level spectra for the as-grown and plasma treated films showed the introduction of new spectral features after plasma treatment which were attributed to doping of nitrogen into the graphitic lattice and some surface functionalisation. This was confirmed through analysis of the N 1s peak of the plasma treated film which showed that the majority of the nitrogen incorporated into the material was present in pyrrolic or pyridinic configurations; the nitrogen was mostly present in the edge planes of the graphitic lattice.

Cyclic voltammetry with the ferri/ferro-cyanide redox probe showed significantly enhanced electron transfer kinetics for N-PyC. This material exhibited clear redox peaks and the peak to peak potential separation (ΔE_p) was used to calculate a homogeneous rate constant of $k^0 = 4.4 \times 10^{-2}$ cm s^{-1}. The enhanced electron transfer of the N-PyC was further confirmed by EIS where the N-PyC was found to exhibit a lower resistance to charge transfer than for the as-grown film. Further electrochemical analysis using the hexaamine ruthenium(III) chloride redox probe indicated that the surface functionalities may themselves under go minor faradaic processes, contributing a pseudocapacitive charge to the voltammetric response.

The enhanced electrochemical performance is attributed to both the greater density of edge plane sites on the N-PyC in conjunction with the presence of highly electrochemically active nitrogen species. Thus, N-PyC represents a low cost material which has potential uses in electrochemical sensing and catalysis applications where it could replace more expensive electrode materials.

Acknowledgements

This work was supported by Science Foundation Ireland (SFI) under contracts No. 08/CE/I1432, PI_10/IN.1/I3030 and the EU under FP7-2010-PPP Green Cars (Electrograph No. 266391). The staff and facilities of the Advanced Microscopy Laboratory (AML) are thanked for assistance in electron microscopy.

References

1 R. L. McCreery, *Chem. Rev.*, 2008, **108**, 2646–2687.
2 P. Chen and R. L. McCreery, *Anal. Chem.*, 1996, **68**, 3958–3965.
3 K. Kinoshita, *Carbon: electrochemical and physicochemical properties*, John Wiley Sons, New York, NY, 1988.
4 L. Kavan and L. Dunsch, *Electrochemistry of Carbon Nanotubes*, Springer, Berlin, Heidelberg, 2008, vol. 111, pp. 567–603.
5 D. A. C. Brownson and C. E. Banks, *Analyst*, 2010, **135**, 2768–2778.
6 B. Reznik and K. Hüttinger, *Carbon*, 2002, **40**, 621–624.
7 J. Kim, X. Song, K. Kinoshita, M. Madou and R. White, *J. Electrochem. Soc.*, 1998, **145**, 2314–2319.
8 T. Sharifi, F. Nitze, H. R. Barzegar, C.-W. Tai, M. Mazurkiewicz, A. Malolepszy, L. Stobinski and T. Wågberg, *Carbon*, 2012, **50**, 3535–3541.
9 H. Wang, T. Maiyalagan and X. Wang, *ACS Catal.*, 2012, **2**, 781–794.
10 D. Wei, Y. Liu, Y. Wang, H. Zhang, L. Huang and G. Yu, *Nano Lett.*, 2009, **9**, 1752–1758.
11 Y.-C. Lin, C.-Y. Lin and P.-W. Chiu, *Appl. Phys. Lett.*, 2010, **96**, 133110.
12 H. Wang, C. Zhang, Z. Liu, L. Wang, P. Han, H. Xu, K. Zhang, S. Dong, J. Yao and G. Cui, *J. Mater. Chem.*, 2011, **21**, 5430.
13 L. Qu, Y. Liu, J.-B. Baek and L. Dai, *ACS Nano*, 2010, **4**, 1321–1326.

14 J. C. Carrero-Sánchez, A. L. Elías, R. Mancilla, G. Arrellín, H. Terrones, J. P. Laclette and M. Terrones, *Nano Lett.*, 2006, **6**, 1609–1616.
15 S. Deng, G. Jian, J. Lei, Z. Hu and H. Ju, *Biosens. Bioelectron.*, 2009, **25**, 373–377.
16 Y. Wang, Y. Shao, D. W. Matson, J. Li and Y. Lin, *ACS Nano*, 2010, **4**, 1790–1798.
17 E. Raymundo-Piñero, D. Cazorla-Amorós and A. Linares-Solano, *Carbon*, 2003, **41**, 1925–1932.
18 C.-M. Yang and K. Kaneko, *J. Colloid Interface Sci.*, 2002, **255**, 236–240.
19 N. McEvoy, N. Peltekis, S. Kumar, E. Rezvani, H. Nolan, G. P. Keeley, W. J. Blau and G. S. Duesberg, *Carbon*, 2012, **50**, 1216–1226.
20 J. L. Ely, M. R. Emken, J. A. Accuntius, D. S. Wilde, A. D. Haubold, R. B. More and J. C. Bokros, *J. Heart Valve Dis.*, 1998, **7**, 626–632.
21 S. Behzadi, M. Imani, M. Yousefi, P. Galinetto, A. Simchi, H. Amiri, P. Stroeve and M. Mahmoudi, *Nanotechnology*, 2012, **23**, 045102.
22 A. Koster, H. D. Matzner and D. R. Nicholsi, *Nucl. Eng. Des.*, 2003, **222**, 231–245.
23 A. P. Graham, G. Schindler, G. S. Duesberg, T. Lutz and W. Weber, *J. Appl. Phys.*, 2010, **107**, 114316.
24 H.-Y. Kim, K. Lee, N. McEvoy, C. Yim and G. S. Duesberg, *Nano Lett.*, 2013, **13**, 2182–2188.
25 A. P. Graham, K. Richter, T. Jay, W. Weber, S. Knebel, U. Schröder and T. Mikolajick, *J. Appl. Phys.*, 2010, **108**, 104508.
26 M. Hadi, A. Rouhollahi and M. Yousefi, *J. Appl. Electrochem.*, 2012, **42**, 179–187.
27 T. Kwon, H. Nishihara, H. Itoi, Q.-H. Yang and T. Kyotani, *Langmuir*, 2009, **25**, 11961–11968.
28 R. Liu, D. Wu, X. Feng and K. Müllen, *Angew. Chem.*, 2010, **122**, 2619–2623.
29 G. Keeley, N. McEvoy, S. Kumar, N. Peltekis, M. Mausser and G. Duesberg, *Electrochem. Commun.*, 2010, **12**, 1034–1036.
30 G. P. Keeley, N. McEvoy, H. Nolan, S. Kumar, E. Rezvani, M. Holzinger, S. Cosnier and G. S. Duesberg, *Anal. Methods*, 2012, **4**, 2048–2053.
31 N. McEvoy, H. Nolan, N. Ashok Kumar, T. Hallam and G. S. Duesberg, *Carbon*, 2013, **54**, 283–290.
32 N. Peltekis, S. Kumar, N. McEvoy, K. Lee, A. Weidlich and G. S. Duesberg, *Carbon*, 2012, **50**, 395–403.
33 N. A. Kumar, H. Nolan, N. McEvoy, E. Rezvani, R. L. Doyle, M. E. G. Lyons and G. S. Duesberg, *J. Mater. Chem.*, 2013, **1**, 4431–4435.
34 X. Mei and J. Ouyang, *Carbon*, 2011, **49**, 5389–5397.
35 H. L. Poh, F. Šaněk, A. Ambrosi, G. Zhao, Z. Sofer and M. Pumera, *Nanoscale*, 2012, **4**, 3515.
36 O. C. Compton, D. A. Dikin, K. W. Putz, L. C. Brinson and S. T. Nguyen, *Adv. Mater.*, 2010, **22**, 892–896.
37 D. Sun, X. Yan, J. Lang and Q. Xue, *J. Power Sources*, 2013, **222**, 52–58.
38 A. L. M. Reddy, A. Srivastava, S. R. Gowda, H. Gullapalli, M. Dubey and P. M. Ajayan, *ACS Nano*, 2010, **4**, 6337–6342.
39 Y. Shao, S. Zhang, M. Engelhard, G. Li, G. Shao, Y. Wang, J. Liu, I. Aksay and Y. Lin, *J. Mater. Chem.*, 2010, **20**, 7491–7496.
40 X. Li, H. Wang, J. T. Robinson, H. Sanchez, G. Diankov and H. Dai, *J. Am. Chem. Soc.*, 2009, **131**, 15939–15944.
41 J. Kim, D. Jung, Y. Park, Y. Kim, D. W. Moon and T. G. Lee, *Appl. Surf. Sci.*, 2007, **253**, 4112–4118.
42 B. Ruelle, S. Peeterbroeck, R. Gouttebaron, T. Godfroid, F. Monteverde, J.-P. Dauchot, M. Alexandre, M. Hecq and P. Dubois, *J. Mater. Chem.*, 2006, **17**, 157–159.
43 X. Ji, C. E. Banks, A. Crossley and R. G. Compton, *ChemPhysChem*, 2006, **7**, 1337–1344.
44 K. K. Cline, M. T. McDermott and R. L. McCreery, *J. Phys. Chem.*, 1994, **98**, 5314–5319.
45 R. S. Nicholson, *Anal. Chem.*, 1965, **37**, 1351–1355.
46 M. E. G. Lyons and G. P. Keeley, *Sensors*, 2006, **6**, 1791–1826.
47 J. E. Randles, *Discuss. Faraday Soc.*, 1947, **1**, 11–19.
48 R. J. Rice and R. L. McCreery, *Anal. Chem.*, 1989, **61**, 1637–1641.
49 S. Ranganathan, R. McCreery, S. M. Majji and M. Madou, *J. Electrochem. Soc.*, 2000, **147**, 277–282.